Journal of The Electrochemical Society

Avoiding Thermal Issues During Fast Charging Starting with Proper Cell Selection Criteria

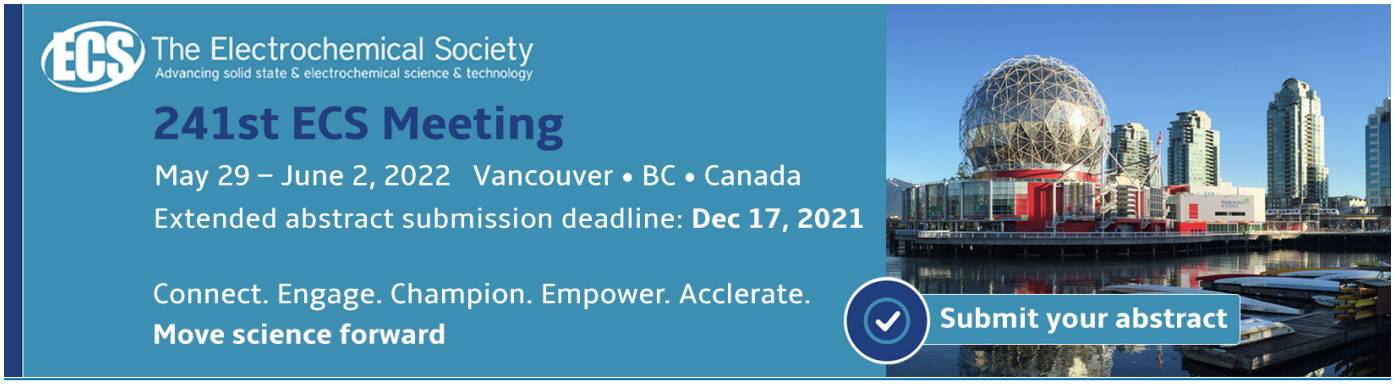

Journal of The Electrochemical Society, 2021 **168** 110523

Avoiding Thermal Issues During Fast Charging Starting with Proper Cell Selection Criteria

Eneko Gonzalez-Aguirre,[1,2,z] Jon Gastelurrutia,[1] Mahesh Suresh Patil,[3] and Luis del Portillo-Valdes[2]

[1]*IKERLAN Technology Research Centre, Basque Research and Technology Alliance (BRTA), 20500 Arrasate/Mondragón, Spain*
[2]*Energy Engineering Department, University of the Basque Country (UPV/EHU), Engineering School of Bilbao, Spain*
[3]*Research Group MOBI—Mobility, Logistics, And Automotive Technology Research Centre, Vrije Universiteit Brussel, Brussels 1050, Belgium*

Proper cell selection is determinant to optimize systems and reduce risks for new and high demanding areas such as electromobility. Thermal performance must be an indispensable selection criterion to avoid thermal issues in these fields, so cells should be correctly characterised and modelled. In this paper, an improved cell selection methodology that focuses on the thermal performance criterion especially for fast charging applications is proposed. After a first selection, two cell candidates were characterised and their heat generation was modelled and compared. With the selected cell, heat generation rate was determined and a 3C fast charge was performed to evidence the predicted thermal performance. The improved methodology identified a cell with an advantageous entropic heat coefficient (EHC) for fast charging, decreasing the heat energy generation by 54% concerning the other candidate cell, which results in optimisation of the thermal management system (TMS). This emphasizes the importance of proper cell selection based on thorough thermal characterization.
 [DOI: 10.1149/1945-7111/ac3348]

Manuscript submitted July 22, 2021; revised manuscript received October 1, 2021. Published November 15, 2021.

List of symbols

$\dot{Q}$	Heat generation/consumption rate [W]
η_{charge}	Efficiency at charge [%]
$C_{p_{avg}}$	Average Specific Heat Capacity [$Jkg^{-1}K^{-1}$]
E_{charge}	Electrical Energy Charged [kWh]
I	Current [A]
M	Cell mass [kg]
n_{cell}	Number of cells
Q_{irr}	Irreversible Heat Energy [kWh]
R_{in}	Internal Resistance [Ω]
T	Temperature [K]
t	Time [s]
U^{avg}	Equilibrium potential—evaluated at volume-averaged concentration [V]

The electrification of the transport sector is a real fact settling nowadays with the increase of electric vehicles (EV) and hybrid electric vehicles (HEV) in our cities, boosted by the legislative aim of reducing greenhouse gas emissions.[1] For this purpose, the lithium-ion (Li-Ion) battery is a promising and widely used technology, because of its large power storage capacity, good energy density/weight ratio, no memory effect and high efficiency of 90%–100%.[2] However, a great potential of overheating is the main problem of these batteries, with operating temperature and temperature differences between the cells being closely related to their performance and durability.[1,3]

Moreover, whereas the acceptable operating temperature range for the Li-Ion batteries is –20°C to 60°C, the recommended working temperature to maintain its optimal performance is between 20°C and 40°C, with a maximum difference of 5°C.[4] Due to extra heat generation, the fast-charging target makes overheating a real issue for reliability and security. High charging C-rates have been shown to accelerate degradation, deteriorating the capacity and power capabilities of batteries.[5] To reduce this thermal stress, more powerful TMSs are being implemented. Nevertheless, these systems suppose great auxiliary consumption, extending the plugged periods and reducing the system's efficiency. The usage of passive systems such as phase change materials (PCM) or even immersion cooling is also considered,[6] but extra weight is added to the system and at the end, the active part of the TMS takes charge of dissipating the stored latent heat.[7]

Choosing the battery cells with an adequate thermal behavior could handle this problem by reducing the energy consumption of TMS and lowering the total weight of the battery pack (BP). This entails an overall efficiency and reliability increase, especially concerning fast-charging operations. For that purpose, the thermal behavior of battery cells needs to be studied in depth. Accurate characterization and analysis are necessary to predict the heat generation and use the data to avoid any issues of overheating, TMS over-sizing or under-sizing and to cover precisely the cooling needs.

Regarding batteries' thermal characterization, Bernardi et al.[8] defined heat generation on a cell by irreversible and reversible heat. The first one refers to joule heating and always represents exothermic heat generation. However the latter is referred to as entropic heat due to entropy changes and behaves asymmetrically during charge and discharge, changing its thermal behavior from exothermic to endothermic regarding cell's state of charge (SOC). These heat generation terms constitute the main heat power of a cell and are represented respectively as a sum on Eq. 1

$$\dot{Q} = I^2 \cdot R_{in} + I \cdot T \cdot \frac{\partial U^{avg}}{\partial T} \qquad [1]$$

where I [A] is the cell charging (positive) or discharging (negative) current, R_{in} [Ω] is the internal resistance of the cell, T [K] is cell's temperature and $\partial U^{avg} \cdot \partial T^{-1}$ [VK^{-1}] is the Entropic Heat Coefficient (EHC) defined by equilibrium potential changes to temperature.

On the thermal characterisations shown in literature, a lack of uniformity when analysing both reversible and irreversible heat is found. The most considered term is irreversible heat, which behaves

[z]E-mail: eneko.gonzalez@ikerlan.es

as an exothermic process regardless of whether the cell is charging or discharging. To evaluate this irreversible heat, the internal resistance of the battery cell needs to be characterised. It is sometimes determined only as a function of the state of charge[9] or as a function of temperature,[10] but usually both terms are considered when obtaining it.[11–15]

Regarding reversible heat, the EHC is what defines the exothermic or endothermic performance and amount of heat for each SOC step on charge and discharge processes. At positive EHC values, a cell will generate heat on charge (positive current value) whereas it will absorb on discharge (negative current value). The opposite happens with negative EHC values. Thus, reversible heat creates an asymmetric thermal behavior whether charge and discharge operations are compared for the same C-rate. Therefore, and as it tends to be smaller than the irreversible one, there is an underestimation of the reversible heat. Sometimes is directly neglected for a supposed imperceptible effect,[9,10] or is not even mentioned.[16] Other studies do not truly consider it[11,17,18] or it is used on their models but with a low impact.[19–21] Finally, some authors are recognizing the effect of entropy changes on the heat generation process,[12,15,22] whereas some others emphasize the importance of further studying it due to the great percentage of reversible heat out of the total heat generated.[13,14,23,24]

EHC changes are subjected to each cell, so it should be studied on every characterization to determine its importance. Furthermore, the EHC comparison over cell chemistries shows different tendencies for Lithium Nickel Manganese Cobalt Oxide (NMC), Lithium Iron Phosphate (LFP) and Lithium Titanate Oxide (LTO) cells. As shown in Fig. 1, both NMC and LFP cells have a positive rise on half of the charge whereas LTO cells are flatter with very low or even negative values all over the SOC. This will minimize the reversible heat generation during cell cycling.

In addition to reversible heat underestimation and as far as it has been observed in the literature, there is not a clearly defined methodology on cell selection criteria for fast charging along with thermal behavior. The established methodology is based on tests to measure and validate cell characteristics, ageing and lifetime, safety or even cost parameters, but thermal behavior is rarely accounted for Refs. 34, 35. Some studies take into consideration the operating temperature for technology selection or storage system sizing[36,37] and even the effect of the state of charge, capacity and ageing on thermal behavior is considered,[38] but a gap can be clearly found on cell selection methodologies for thermal behavior and especially for fast charging issues.

This work seeks to solve the problems mentioned above by proper cell selection inside an electrification project of an already existing internal combustion engine vehicle (ICE). The cell selection for this particular application and the battery pack construction are the most important tasks of the project. For successful development of the job, on this work, an already existing cell selection methodology focused, especially on ageing and lifetime[35,39] is extended and improved with further analysis of the thermal behavior. This will lead to optimization of selection criteria by avoiding thermal issues, with particular emphasis on cell's fast charging, as this has become a considerably more demanding process than normal driving discharge on EVs.

During the selection process, two candidates are selected from the initial cell samples owing to battery pack requirements and cell specifications for the desired application. Then, both of them are thermally characterised following the improved methodology and their heat potential is compared selecting the most suitable one for the application. To emphasize the selected cell's proper heat behavior, heat generation rate is evaluated in an adiabatic environment. Finally, the fast charging behavior of the selected cell is also experimentally analysed to stress the importance of the results obtained.

Improved Cell Selection Methodology

The optimization of cell selection methodology needs the inclusion of a deeper thermal behavior analysis so overheating especially when fast charging can be avoided. The improved cell selection methodology presented in this work is based on a previous approach currently used[35] and specially focused on electrical performance.

Original methodology.—This base methodology is divided into different stages:

Stage 0: Li-Ion cell market database.
Stage 1: (a) Analysis of the application and battery pack requirements.
(b) Identification and theoretical assessment of suitable cell's technical specifications.
Stage 2: Cell characterization: nominal capacity, rate capability and internal resistance validation tests and accelerated life cycle tests.
Stage 3: Calendar and cycle ageing and lifetime, safety and cost analysis.

The stages above summarize the necessary methodology to select a cell from a large database. Stage 1 is essential for getting a fast and enough reduced cell candidate list by comparing the application requirements with the available cells' characteristics selected from the Stage 0 database. With few candidate cells, stage 2 then characterises them under application conditions especially focusing on cell manufacturer's data validation. Finally, at stage 3, durability, cost and safety analysis of the selected cell is carried out. Each stage is considerably more time demanding than the previous one, so the candidate amount must be widely reduced at the end of each stage. Therefore, reaching stage 3 with one candidate is highly encouraged as testing time could be significantly reduced.

Improved methodology.—For the implementation of an effective and detailed thermal performance analysis on the new improved methodology, both irreversible and reversible heat must be considered. As explained above, the cell characterisations on stage 2 measure the internal resistance of the cell so the irreversible heat can be already determined. However, the reversible heat is not considered as the entropic heat coefficient is not measured. The

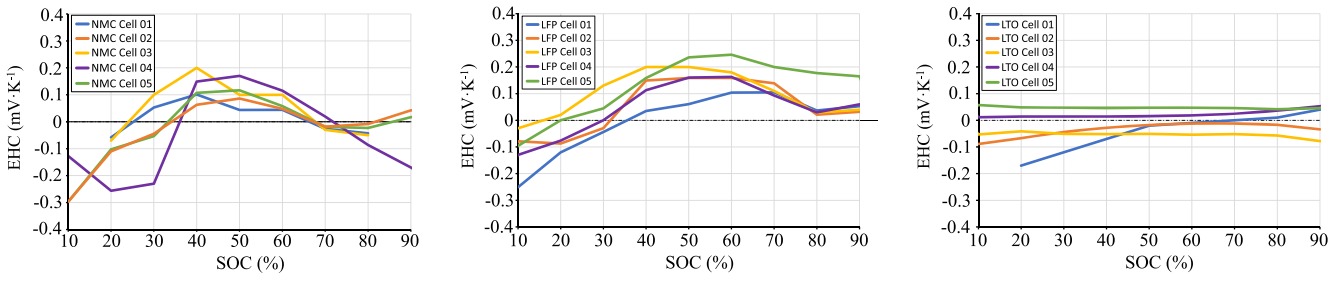

Figure 1. EHC change depending on cell chemistry.[13,15,19,23–33]

importance of that element on the thermal behavior will depend on each cell characteristic, but it is an indispensable factor for a precise thermal analysis. Because of this, both electrical and thermal characterization of the cell must be done at the second stage.

Therefore, EHC must be implemented for the improved methodology, being the second stage the most appropriate as the characterization is done and cell parameters are analysed on it. The new improved methodology arrangement is shown on Fig. 2. An initial approach of 10% of SOC precision is suggested with the possibility of deepening accuracy to 5% on exceptional and interesting SOC locations. Even the most exhaustive analysis of EHC will not exceed more than two weeks from the three months designated for both Stage 1 and 2 on the original methodology, hence is an acceptable and affordable period. The accelerated life cycle test is now comprehended by ageing and lifetime tests of Stage 3, which remains as it was defined in the originally proposed methodology.

For a right comparison between different cells' heat generation, some common criteria must be defined. Thus, the application requirements are used as the basis. First of all, based on application BP's minimum necessary energy, cell series-parallel arrangement is proposed determining the cell number to be used. This cell amount is then implemented on the thermal model, extrapolating the cell's heat generation for the complete battery pack. Moreover, the fast charging criterion is also important. In this case, time is taken as an invariable factor, so a determined C-rate is used to charge all candidate cells. Therefore, the same energy quantity is supposed to be recharged for the battery pack, so time and energy requirements are fulfilled for the application, providing a fair comparison between different cells.

This improved methodology will introduce the cell's thermal behavior as a parameter when selecting the cell. The lowest heat generation especially on fast charging will succeed on the comparison for this criterion. Moreover, an endothermic behavior will be the performance looked for, as it will lead to a temperature decrease.

Once the needed cell properties and comparison criteria are identified for the improvement of the cell selection methodology, the next Section presents the implementation of this methodology for the cell selection done in this work.

Cell Selection Analysis and Results

This Section follows the improved methodology to choose the most appropriate cell for the ICE vehicle electrification project.

Stage 0 results.—At this stage, candidate cells were searched on the database. As a result, five available samples were identified and selected showing their technical specifications on Table I. Due to large differences in specifications, suitability with this project will be determined in the next stage.

Stage 1 results.—This stage assesses the conformity between the application's battery pack requirements and candidate cells' specifications. The project is based on three main requisites: required energy, maximum available volume and minimum necessary fast-charging capacity. A minimal cell lifetime is also needed to ensure the project's viability.

The battery pack's energy amount, which must surpass 30 kWh, is a mandatory vehicle capability to achieve the desired autonomy. Moreover, on account of this is the electrification of an originally ICE vehicle, the available space for the battery pack is limited to 220 litres. Furthermore, fast charging of the vehicle is the other essential requisite for the application, being a 3C charge the standard minimum. Finally, a minimum lifetime of 1500 cycles is demanded on the project.

With these references, arrangements for a battery pack above 30 kWh are considered with all candidate cells. BP's voltage is also attempted to be around 400V, pursuing some standardization. The resulting cell series-parallel configuration and the number of cells (n_{cell}) used is shown on Table II, also determining the outcome volume. Cells' charging C-rate is as well compared with the application requisite.

Sample 3 and Sample 5 are below the minimum charging C-rate, while sample 4 exceeds the maximum available volume. All cells have a higher lifetime than the minimum defined for the application. Therefore samples 1 and 2 are the candidate cells to analyze on stage 2 of the improved methodology.

The charging current to be used in this work is determined by the lowest C-rate of Sample 2, with the maximum limit of 3C charge. Moreover, to reach the desired battery pack energy, 570 and 204 cells of samples 1 and 2 are used respectively. These values will be introduced on the following thermal model on stage 2, establishing a standard and fair enough comparison of both BP's heat generation.

Stage 2 results.—This second stage is divided into two main assignments, where cell parameters are measured and their heat generation is compared respectively.

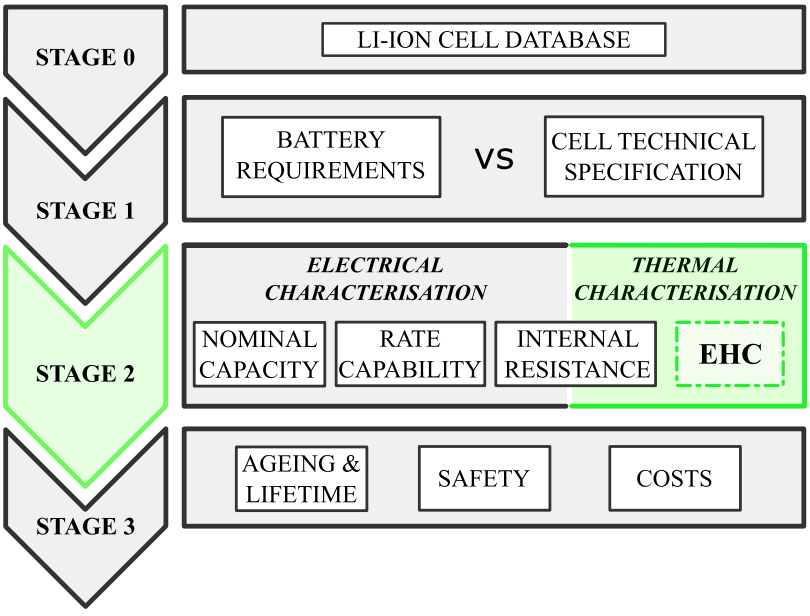

Figure 2. Improved methodology with EHC measurement and thermal characterization.

Table I. Stage 0 candidate cells' specifications.

	Sample				
	1	**2**	**3**	**4**	**5**
Chemistry	LTO	NMC	NMC	LFP	LFP
Nominal Capacity (Ah)	23	40	5	10	50
Nominal Voltage (V)	2.3	3.7	3.6	3.2	3.2
Nominal Energy (Wh)	52.9	148	18	32	160
Specific Energy ($Wh{\cdot}kg^{-1}$)	96	160	267	128	120
Energy Density ($Wh{\cdot}L^{-1}$)	203	288	186	66.3	227.9
Maximum Charge (C-rate)	8C	3C	0.7C	10C	2C
Weight (kg)	0.55	0.99	0.068	0.25	1.329
Volume (L)	0.260	0.513	0.098	0.483	0.702
Lifetime (cycles)	15 000	3000	4000	2500	2000
Geometry	Prismatic	Pouch	Cylindric	Cylindric	Prismatic

Table II. Stage 1 cell selection by application requirements comparison.

	BP	SAMPLE				
	Requisites	**1**	**2**	**3**	**4**	**5**
BP Energy (kWh)	30	30.15	30.19	30.24	30.02	30.72
Voltage (V)	-	437.0	377.4	432.0	428.8	307.2
Cell Configuration	-	190S3P	102S2P	120S14P	134S7P	96S2P
Number of cells (n_{cell})	-	570	204	1680	938	192
Total Volume (L)	Max. 220L	148.2	104.7	164.6	453.1	134.8
Charge (C-rate)	Min. 3C	8C	3C	0.7C	10C	2C
Lifetime (cycles)	Min. 1500	15000	3000	4000	2500	2000

Cell parameter measurement includes nominal capacity, rate capability, internal resistance and entropic heat coefficient. The first two properties characterize the cell electrically pursuing the cell supplier's data validation. The two latter elements characterize the cell thermally. Thus, R_{in} is only evaluated from a thermal perspective in this specific work.

Moreover, in the second part of stage 2, R_{in} and EHC values will allow the cell's heat power estimation by irreversible and reversible heat respectively. Thus, thermal analysis and consequent cell selection will be done by the cell's fast charging evaluation.

Measured cell parameters.—Nominal capacity is measured by 3 charge-discharge cycles at 0.2C and different temperatures using a thermal chamber, while rate capability measures cells' capacity at different current loads.[35] The R_{in} values are measured by constant current discharge pulses of 18 seconds for different SOC and temperature levels,[40] while variable temperature potentiometry is used for EHC measurements.[41]

(a) Nominal Capacity and Rate Capability: temperature and C-rate influence the capacity of the cells considerably. However, cells' nominal specifications must be reached to accept the validity of samples. This nominal capacity values, as shown on Table I, are 23 Ah and 40 Ah for samples 1 and 2 respectively, measured at 25°C and 0.5C testing conditions. On the characterization process, nominal capacity tests were carried out at 10°C, 20°C, 30°C and 40°C at 0.2C, whereas 0.5C, 1C, 2C and 4C tests were done at 25°C for rate capability. As shown on

Table III. Nominal Capacity and Rate Capability of Sample 1 and Sample 2.[42]

Nominal Capacity*(Ah)*				**Rate Capability*(Ah)***	
Temp	Sample 1	Sample 2	**C-Rate**	Sample 1	Sample 2
10°C	22.22	39.39	**0.5C**	23.3	40.3
20°C	23.30	40.43	**1C**	23.1	38.3
30°C	24.03	41.29	**2C**	23.0	38.0
40°C	24.57	41.97	**4C**	22.8	37.6

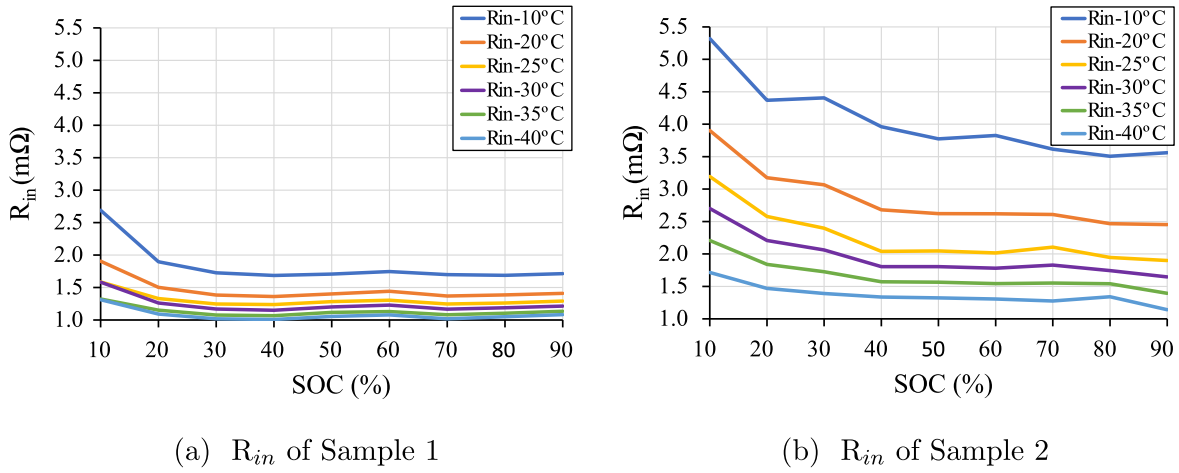

Figure 3. Internal Resistance.

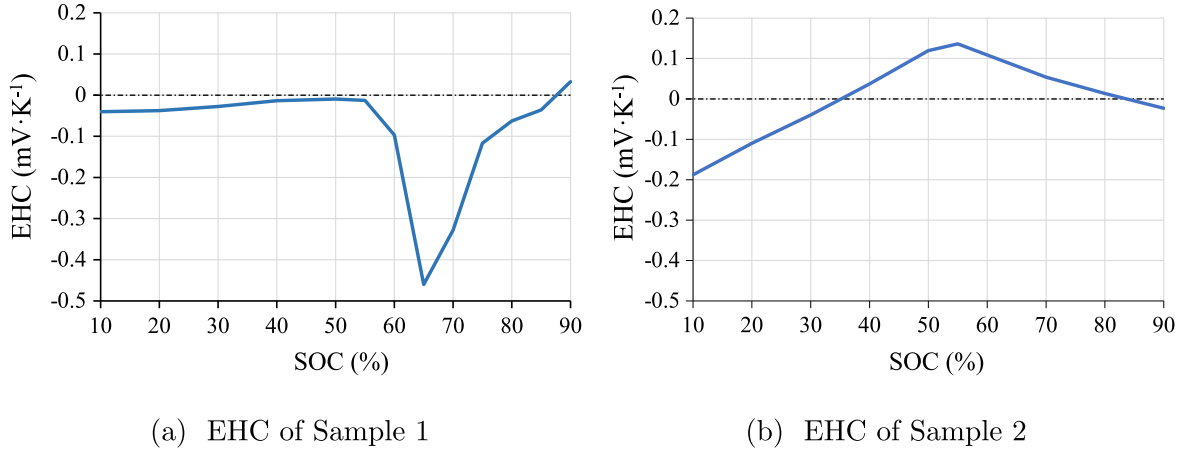

Figure 4. Entropic Heat Coefficient.

Table III, cell manufacturer's data is successfully reached and only deteriorates at cold temperatures (10°C) and high C-rates (>2C for sample 1 and > 1C for sample 2). Therefore cells are valid to be used in this project.

(b) Internal Resistance: the internal resistance is measured from 10% to 90% of cells' SOC with a resolution of 10%. On the other hand, the temperatures of the tests are 10°C, 20°C, 25°C, 30°C, 35°C and 40°C. The Figs. 3a and 3b shows the internal resistance results obtained for sample 1 and 2 respectively. A usual performance of R_{in} with its increase at low SOC levels and temperatures can be seen, but with considerably higher resistance levels on the second cell.

(c) Entropic Heat Coefficient: the entropic heat coefficient of both candidate cells is obtained with a 10% resolution of the SOC, from 10% to 90%. However, 5% accuracy is introduced in areas of quick changes; data at 55% of SOC is added for sample 2 and data steps of 5% are also introduced from 50% to 90% of SOC values for sample 1. As shown on Fig. 4a the EHC of sample 1 candidate cell among all the SOC is quite constant with a pronounced negative peak of -0.46 mVK^{-1} on the 65% of the charge level. This will suppose a heat power increase when discharging the cell at that SOC level, whereas an endothermic effect with the corresponding heat power decrease will occur during the charging process. On the other hand, sample 2 has a negative part with –0.2 mVK^{-1} peak on the initial SOC level which is counteracted with positive EHC values almost on all the rest of the SOC level and a maximum value of 0.13 mVK^{-1} on 55% of SOC.

Heat generation comparison.—The generated heat estimation model used at this second stage follows the procedures established by Nieto et al.[43] complying with the already shown Eq. 1. This heat generation model of the cell was already validated in several works.[43–45] However, the number of cells is added to extrapolate the heat generation to the battery pack level as shown on Eq. 2.

$$\dot{Q} = \left(I^2 \cdot R_{in} + I \cdot T \cdot \frac{\partial U^{avg}}{\partial T}\right) \cdot n_{cell} \qquad [2]$$

The heat generation model is fed with the SOC, which is estimated under the coulomb counting method through nominal capacity,[46] the charging current and a constant and invariable cell temperature inputs. R_{in} and EHC are determined for every time step with those inputs, from the characterization data on *measured cell parameters* section. Heat generation will be higher on the discharge process under the same cycling conditions for samples with prevailing negative EHC values. However, the fast-charging process is substantially more demanding due to higher C-rate usage, which increases the irreversible heat well above the reversible part and therefore the total heat generation. Thus, the thermal model is computed over the cell's charging process

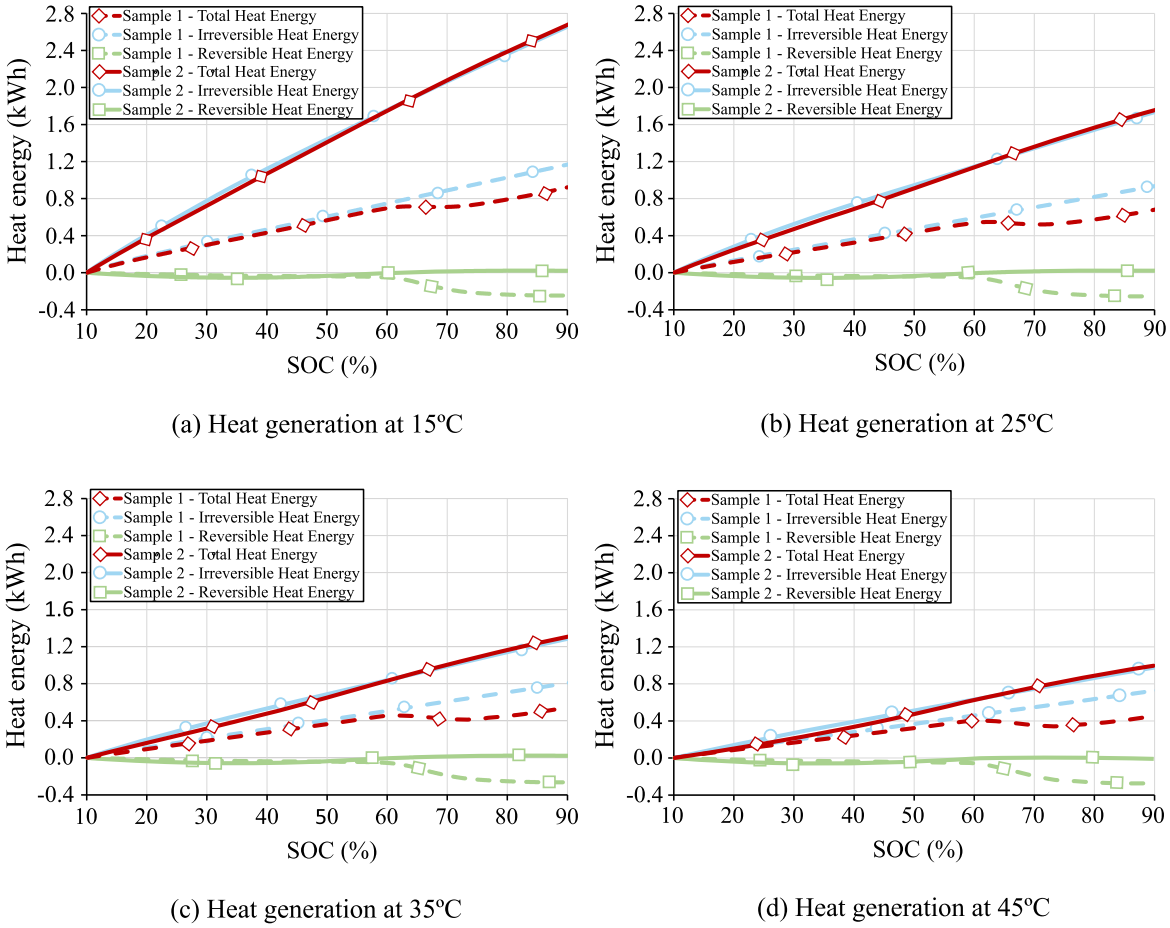

Figure 5. Heat energy generation of sample 1 and 2 at 3C charge.

Table IV. Heat energy generation results at the end of the 3C charge.

Temp	Sample 1*(kWh)*				Sample 2*(kWh)*			
	Q_{irr}	Q_{rev}	Q_{tot}	$\eta_{charge}(\%)$	Q_{irr}	Q_{rev}	Q_{tot}	$\eta_{charge}(\%)$
15°C	1.17	−0.25	**0.93**	**95.1%**	2.67	0.02	**2.69**	**88.9%**
25°C	0.94	−0.26	**0.68**	**96.1%**	1.74	0.02	**1.76**	**92.8%**
35°C	0.81	−0.26	**0.55**	**96.6%**	1.29	0.02	**1.31**	**94.6%**
45°C	0.73	−0.27	**0.46**	**97.0%**	0.98	0.02	**1.01**	**95.9%**

obtaining the correspondent heat energy generation of the most demanding operation part.

For the given application on this work, the heat generation model is fed for a 3C fast charge at four different constant temperatures; 15°C, 25°C, 35°C and 45°C. The reversible, irreversible and total heat energy amount for sample 1 (discontinuous line) and sample 2 (continuous line) cells are compared as shown on Fig. 5. The irreversible energy decreases with higher temperatures due to internal resistance lowering. This effect is more clearly appreciated with cell candidate 2, which has considerably higher R_{in} values at low temperatures.

The reversible energy change is very small in comparison with the irreversible one, so it has little effect when changing the temperature. However, both cells' heat energy amount is very different. As seen on Table IV, sample 2 ends the charge with 20 Wh of reversible heat generation (Q_{rev}), whereas sample 1 even absorbs around 250 Wh. This effect, as seen on the total heat energy generated during charge, helps candidate 1 to reduce its heating capacity, with the consequent temperature reduction. Even at 45°C, with the lowest irreversible generation (Q_{irr}), favourable EHC and thus the reversible heat makes sample 1 release less than half of the total heat than sample 2. This is also supported with the charging energy efficiency values (η_{charge}) obtained from Eq. 3, where only the irreversible heat generation is considered as charge/discharge net reversible heat is zero.[47]

$$\eta_{charge} = \frac{E_{charge} - Q_{irr}}{E_{charge}} \quad [3]$$

E_{charge} [kWh] is related to the electrical energy charged on each battery pack arrangement from 10% to 90% of SOC and Q_{irr} [kWh] is the irreversible heat generation of the process. The higher efficiency shown in sample 1 for all evaluated temperatures is accompanied by an endothermic reversible heat. Therefore, the

energy consumed by the TMS for that heat dissipation will be proportionally lower than necessary for sample 2.

This phenomenon of cell candidate 1 will lead to a better operation with lower final temperatures, so the cooling needs on fast charging will be much lower. Moreover, it facilitates the control and reduces the possible security problems, making this cell the most suitable for this specific application, especially for fast charging operation.

Stage 3 results.—Stage 3 carries ageing and lifetime, safety and cost analysis. Currently, the ageing and lifetime tests are underway for the selected sample after the initial three stages results. However, a longer period will be needed to acquire some consistent results due to the length of the study. Nevertheless, cell manufacturer's data shows to easily comply with project requirements as cells' lifetime seems to be 10 times higher than the minimum defined on the project. Therefore, cell selection outcomes can be provisionally concluded.

Cell selection results.—The cell selection evaluation done along this section, providing that stage 3 results are in concordance with cell manufacturer's ageing and lifetime data, determined Sample 1 to have the most interesting properties among all candidate cells selected on stage 0: 30 kWh battery pack's volume below the maximum available space and up to 8C fast charge ability. Moreover, a restrained heat generation has been characterised at stage 2 even with endothermic zones during the 3C fast charge. Therefore this is the cell selected for this project and the only one examined at the third and final stage as the suppliers ageing, lifetime and safety data fits the application requirements.

Cell's main drawback is the elevated price compared with sample 2 candidates. However, the importance of this factor should be considered in conjunction with its lifetime and security level for making the right decision. Moreover, an important factor in favor of the choice made is the reduced cooling needs as smaller TMS will be needed.

Result Analysis

In this section, cell selection results from the improved methodology are further analysed ratifying the observed favourable behavior of the cell selected. Firstly, the heat generation rate ($\dot{Q}$) is determined through adiabatic calorimetry. Finally, a 3C fast charge is accomplished under three isothermal ambient temperatures. Therefore, the predicted performance of the cell can be verified by temperature measurement under real operation.

Thermal performance during adiabatic ambient discharge.—Heat generation rate determination is done through an adiabatic environment provided by an Accelerating Rate Calorimeter (ARC) with an accuracy of ±0.7%. Reversible heat when charging behaves endothermically due to this particular EHC characteristic and therefore, heat is absorbed by the cell at certain C-rate and SOC levels. As the calorimeter creates an adiabatic environment by heating the enclosure walls and it has no cooling ability, the endothermic processes cannot be precisely tracked. Consequently, the discharge process must be used for generated heat measurement, in which net heat is completely exothermic for this case.

Adiabatic environment ensures no heat transfer to ambient, hence all the heat generated while cell cycling is accumulated on it. In consequence, this energy balance shows two methods to determine the heat generation rate: heat accumulation and heat generation model itself. Both terms are shown on the energy balance equation defined as:

$$I^2 \cdot R_{in} + I \cdot T \cdot \frac{\partial U^{avg}}{\partial T} = MC_{p_{avg}} \frac{dT}{dt} \quad [4]$$

The term on the left side represents the heat generation model presented on Eq. 1. The new term on the right side of the energy balance refers to the heat stored on the cell, where M [kg] is the mass of the cell, $C_{p_{avg}}$ [$Jkg^{-1}K^{-1}$] is the average specific heat capacity and $dTdt^{-1}$ [Ks^{-1}] is the measured temperature change on time.

To obtain the $C_{p_{avg}}$, calorimetry tests had been done.[48] Changing the heat power provided to the cell by a planar resistance, C_p values were obtained by measuring temperature gradient on time. The average value of the tests is used, obtaining 1163 $J \cdot kg^{-1} \cdot K^{-1}$ for the selected cell as shown on Table V.

During adiabatic calorimetry test for $\dot{Q}$ determination, the battery was connected to a programmable cycler (Industrial Battery Tester (IBT) with ±0.1% accuracy of full scale, which runs with Digatron/Firing Circuits BTS-600 software for data evaluation) for discharging the battery at different C-rates. Moreover, an Agilent 34 970A data acquisition system and T-type thermocouples were used to measure the temperature of the cell's surface. The accuracy specifications of the Agilent are ±0.0035% of reading and 0.0005% of range for voltage. Moreover temperature accuracy of Agilent is ±0.5°C of range and 0.2% of reading and the type-T thermocouple has ±1.5°C accuracy. The discharge test setup inside the calorimeter is shown on Fig. 6.

Every test was carried out from 90% to 10% SOC on three different discharging currents of 1C, 2C and 3C. The initial temperature was the ambient one with 22.5°C, 25.5°C and 22.2°C mean values for each test respectively. After the tests, cell temperatures were 31.7°C, 39.8°C and 41.1°C, so more tests at higher discharge current rates were discarded to ensure the cell's performance inside the optimal temperature range. Employing the temperature evolution data registered on cell's adiabatic calorimetry discharge, heat generation was determined by both accumulation and generation equations. These results were plotted into Fig. 7.

The heat generation model's uncertainty is negligible owing to voltage measurement accuracy of Agilent on HTTP and potentiometry tests during cell's R_{in} and EHC parameter characterization. Calorimetry test on $C_{p_{avg}}$ assessment results in considerable uncertainties, hence the uncertainty band of the heat accumulation estimation of three discharge tests is presented in Fig. 7. All the uncertainties were calculated following the methodology established by Lee et al.[49].

Heat power peak due to the minimum EHC value of –0.46 mVK^{-1} is identified on the three discharge tests by both accumulation and generation equations. On that point, reversible heat becomes much bigger increasing the overall heat generation. For the rest of SOC levels, the low EHC value together with a flat internal resistance makes the heat generation quite constant. These results show the special thermal performance of the selected sample 1, which will be considerably beneficial in the charging operation, due to the reversible heat flip.

Thermal performance during isothermal ambient charge.—At this part, the identified favourable thermal behavior of the selected cell has been further analysed by fast charging. This way, the predicted operation and optimal thermal response observed during cell selection can be studied and verified on the real operation.

The thermal model forecasts an optimistic scenario of punctual heat power reduction below zero with consequent temperature decrease on fast charging if the theoretical behavior of EHC is met. To evidence this behavior, a 3C constant fast charge is

Table V. C_p values and test data for cell sample 1.

	P (W)	ΔT_{avg} (°C)	C_p ($J \cdot kg^{-1} \cdot K^{-1}$)	$C_{p_{avg}}$ ($J \cdot kg^{-1} \cdot K^{-1}$)
Sample 1	4.9	22.7	1161	**1163**
	18.7	22.2	1165	

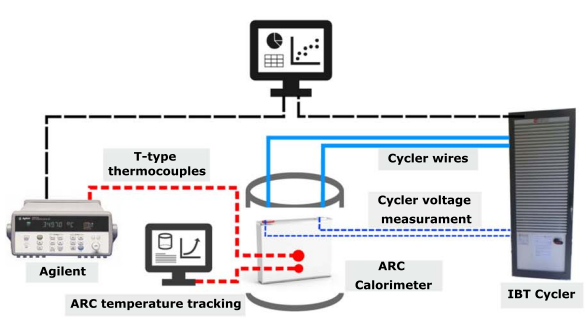

(a) Scheme of calorimetry test.

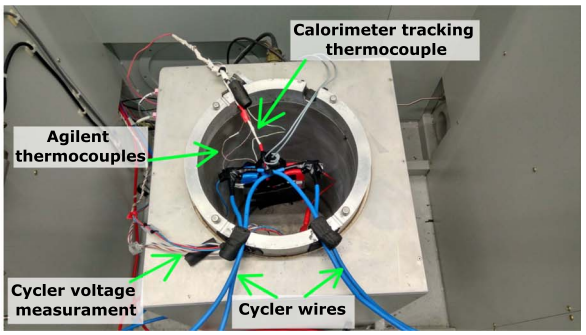

(b) Setup of calorimetry test.

Figure 6. Scheme and setup of adiabatic calorimetry test.

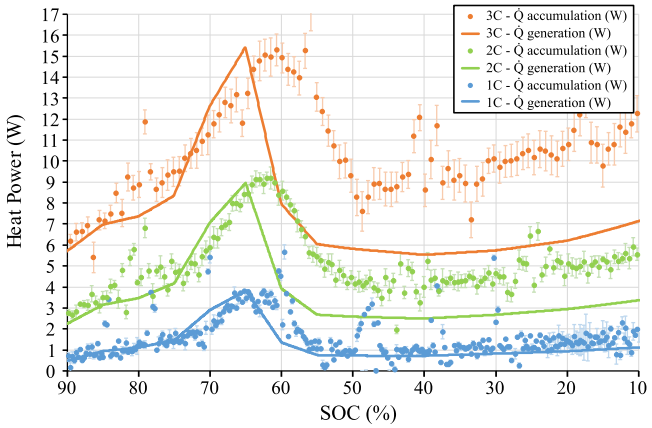

Figure 7. Adiabatic heat power generation analysis by heat accumulation and heat generation methods at 1C, 2C and 3C.

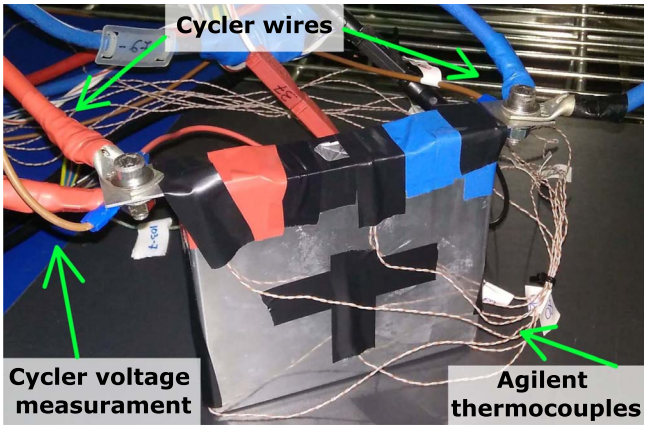

Figure 8. Experimental Setup for fast charge analysis.

performed on a thermal chamber settling three different constant ambient temperatures of 15°C, 25°C and 35°C. Used thermal chamber (CTS, Clima Temperatur Systeme) has an accuracy of ±0.3 K to maintain the desired ambient temperature. Temperature mapping of the cell was done using the Agilent and one T-type thermocouple for each cell surfaces and the IBT was used to charge the cells at 3C current as shows the experimental set-up at Fig. 8.

Due to the high thermal inertia of the cell together with previous slow discharging for the conditioning, the three tests started at slightly higher but stable cell temperatures of 16°C, 26.5°C and 36.1°C respectively. The charge started with the cell fully discharged and stopped when the cell's maximum cut off voltage was reached. Owing to the high charging current, the available capacity of the cell decreased significantly and cut off voltage was reached before completely charging it. The temperature also influenced this behavior as the internal resistance is lower and allows charging more energy at high temperatures. Therefore, only 77% of SOC is charged at 15°C, 88% at 25°C, and even 92% of SOC is reached at 35°C test.

Reached surface mean cell temperatures at the end of the three tests were 21.8°C, 32.8°C and 40.3°C respectively, so cell's performance inside optimal temperature range was guaranteed just with the constant ambient temperature. For better result comparison between tests and to emphasize ambient temperature importance, the cell's temperature difference evolution regarding test initial temperature is shown in Fig. 9. The effect of reversible heat is highly noticeable, with an important temperature fluctuation at 60%–75% of SOC. Temperature reductions are quite small with a decrease of 0.21°C, 0.17°C and 0.41°C respectively. However, this variation provides a considerable stabilisation of the temperatures and an important decrease in the final cell's maximum temperature.

Conclusions

An improved battery cell selection methodology focused on thermal behavior criterion is presented and applied to a real cell selection case. The previous methodology was only based on electrical and ageing factors comparison. Instead, with the new criterion, the thermal performance of the cell can also be considered as an important selection factor, especially thinking about fast charging needs. For accomplishing this, the importance of considering both internal resistance and entropic heat coefficient is emphasized in this work.

Two candidate cells reached the thermal comparison on this real case study. Both cells were characterised, their heat generation when fast charging was estimated with a heat generation model and the most suitable cell was selected. Moreover, with the chosen cell, heat generation rate was estimated by adiabatic calorimetry and finally, a fast charge test was performed. Both tests proved the predicted performance.

Regarding thermal criterion, sample 1 was selected for its particular endothermic performance on 60%–75% of SOC level. The estimated heat generation was significantly lower, reducing at least 550 Wh from the total heat compared with the other candidate cell. Therefore, the selected cell's efficiency is above the fellow candidate over all the studied conditions. The particular EHC coefficient for fast charging is the essential key of this performance in cell sample 1, demonstrating the methodology presented at this work and the thermal analysis as indispensable factors for a better cell selection.

To sum up, this improved methodology helps in determining the real performance of a battery and giving important selection criteria for choosing the best cell possible for each task. Moreover, the importance of correctly characterising the cell is emphasized after proving the considerable effect the entropic heat coefficient can have

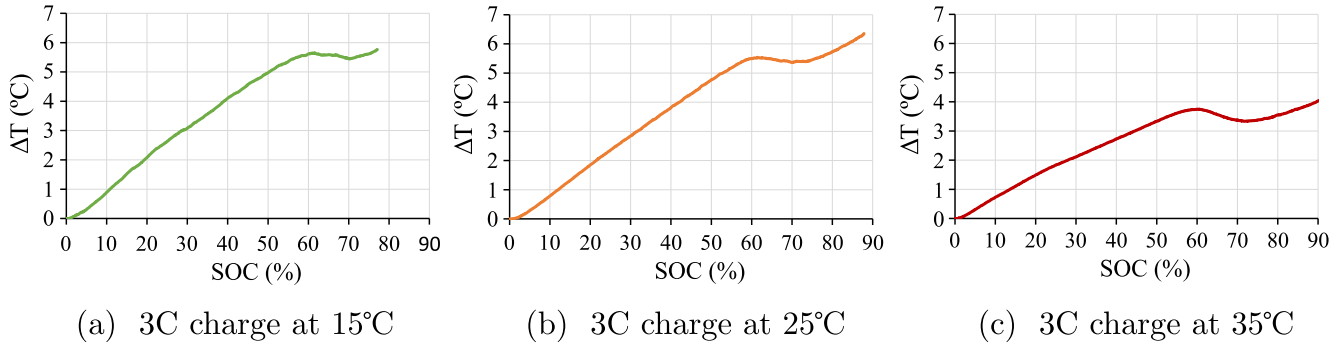

Figure 9. Selected cell's surface mean temperature evolution at 3C charge with 15°C, 25°C and 35°C ambient temperature.

on heat generation performance. This will lead to a better cell selection for such demanding jobs as fast charging, with the consequent TMS reduction, battery pack's efficiency increase and avoidance of any later thermal issues.

Acknowledgments

This paper was developed under the framework of the SELFIE project. This project has received funding from the European Union's Horizon 2020 research and innovation programunder Grant Agreement Nr. 824290 (https://eu-project-selfie.eu/).

ORCID

Eneko Gonzalez-Aguirre https://orcid.org/0000-0002-2861-1810

References

1. S. Manzetti and F. Mariasiu, *Renew. Sustain. Energy Rev.*, **51**, 1004 (2015).
2. M. A. Hannan, M. M. Hoque, A. Mohamed, and A. Ayob, *Renew. Sustain. Energy Rev.*, **69**, 771 (2017).
3. R. Zhao, S. Zhang, J. Liu, and J. Gu, *Journal of Power Sources*, **299**, 557 (2015).
4. A. A. Pesaran, *Journal of Power Sources*, **110**, 377 (2002).
5. A. Tomaszewska et al., *eTransportation*, **1**, 100011 (2019).
6. W. Q. Li, Z. G. Qu, Y. L. He, and Y. B. Tao, *Journal of Power Sources*, **255**, 9 (2014).
7. Siddique A.R.M., S. Mahmud, and B. Van Heyst, *Journal of Power Sources*, **401**, 224 (2018).
8. D. Bernardi, E. Pawlikowski, and J. Newman, *J. Electrochem. Soc.*, **132**, 5 (1985).
9. D. Kang, P. Y. Lee, K. Yoo, and J. Kim, *Journal of Energy Storage*, **27**, 101017 (2020).
10. Y. Ma, Y. Cui, H. Mou, J. Gao, and H. Chen, *Applied Thermal Engineering*, **168**, 114816 (2020).
11. Y. Xie, X. Jing He, X. Song Hu, W. Li, Y. Jun Zhang, B. Liu, and Y. Tao Sun, *Applied Thermal Engineering*, **164**, 114455 (2020).
12. F. Geifes, C. Bolsinger, P. Mielcarek, and K. P. Birke, *Journal of Power Sources*, **419**, 148 (2019).
13. C. Veth, D. Dragicevic, and C. Merten, *Journal of Power Sources*, **267**, 760 (2014).
14. K. E. Thomas and J. Newman, *J. Electrochem. Soc.*, **150**, A176 (2003).
15. G. Vertiz, M. Oyarbide, H. Macicior, O. Miguel, I. Cantero, P. Fernandez De Arroiabe, and I. Ulacia, *Journal of Power Sources*, **272**, 476 (2014).
16. Y. Li, F. Qi, H. Guo, Z. Guo, M. Li, and W. Wu, *Case Studies in Thermal Engineering*, **13**, 100387 (2019).
17. Y. Tang, L. Wu, W. Wei, D. Wen, Q. Guo, W. Liang, and L. Xiao, *Applied Thermal Engineering*, **137**, 11 (2018).
18. Z. An, L. Jia, L. Wei, C. Dang, and Q. Peng, *Applied Thermal Engineering*, **137**, 792 (2018).
19. W. Mei, Q. Duan, C. Zhao, W. Lu, J. Sun, and Q. Wang, *International Journal of Heat and Mass Transfer*, **148**, 119082 (2020).
20. P. Lyu, Y. Huo, Z. Qu, and Z. Rao, *Applied Thermal Engineering*, **166**, 114749 (2020).
21. B. Wang, C. Ji, S. Wang, J. Sun, S. Pan, D. Wang, and C. Liang, *Applied Thermal Engineering*, **168**, 114831 (2020).
22. M. Xu, R. Wang, B. Reichman, and X. Wang, *Journal of Energy Storage*, **20**, 298 (2018).
23. C. Forgez, D. Do Vinh, G. Friedrich, M. Morcrette, and C. Delacourt, *Journal of Power Sources*, **195**, 2961 (2010).
24. A. Eddahech, O. Briat, and J. M. Vinassa, *Energy*, **61**, 432 (2013).
25. Y. Hu, S. Y. Choe, and T. R. Garrick, *Electrochimica Acta*, **362**, 137124 (2020).
26. M. Balasundaram, V. Ramar, C. Yap, L. Lu, A. A. Tay, and B. Palani, *Journal of Power Sources*, **328**, 413 (2016).
27. V. V. Viswanathan, D. Choi, D. Wang, W. Xu, S. Towne, R. E. Williford, J. G. Zhang, J. Liu, and Z. Yang, *Journal of Power Sources*, **195**, 3720 (2010).
28. Z. Geng, J. Groot, and T. Thiringer, *IEEE Transactions on Transportation Electrification*, **6**, 257 (2020).
29. S. Du, M. Jia, Y. Cheng, Y. Tang, H. Zhang, L. Ai, K. Zhang, and Y. Lai, *International Journal of Thermal Sciences*, **89**, 327 (2015).
30. T. M. Bandhauer, S. Garimella, and T. F. Fuller, *Journal of Power Sources*, **247**, 618 (2014).
31. K. Jalkanen and K. Vuorilehto, *Journal of Power Sources*, **273**, 351 (2015).
32. S. S. Madani, E. Schaltz, and S. K. Kæ, *Energies*, **12**, 2685 (2019).
33. P. Schröer, H. van Faassen, T. Nemeth, M. Kuipers, and D. U. Sauer, *Journal of Energy Storage*, **28**, 101189 (2020).
34. K. Chen, F. Zhao, H. Hao, and Z. Liu, *10th International Conference on Applied Energy (ICAE 2018)*, **158** (2019).
35. E. Sarasketa-Zabala, "A novel approach for Li-ion battery selection and lifetime prediction." *Ph.D. Thesis*, Goi Eskola Politeknikoa, Mondragon (2014).
36. T. Sayfutdinov, M. Ali, and O. Khamisov, *Electric Power Systems Research*, **185**, 106388 (2020).
37. V. Vega-Garita, A. Hanif, N. Narayan, L. Ramirez-Elizondo, and P. Bauer, *Journal of Power Sources*, **438**, 227011 (2019).
38. Y. F. Wu, D. Brun-Buisson, S. Genies, F. Mattera, and J. Merten, *ECS Trans.*, **16**, 93 (2019).
39. E. Sarasketa-Zabala, I. Gandiaga, E. Martinez-Laserna, L. M. Rodriguez-Martinez, and I. Villarreal, *Journal of Power Sources*, **275**, 573 (2015).
40. H. G. Schweiger, O. Obeidi, O. Komesker, A. Raschke, M. Schiemann, C. Zehner, M. Gehnen, M. Keller, and P. Birke, *Sensors*, **10**, 5604 (2010).
41. K. E. Thomas, C. Bogatu, and J. Newman, *J. Electrochem. Soc.*, **148**, A570 (2001).
42. T. Kalogiannis, M. S. Hosen, M. A. Sokkeh, S. Goutam, J. Jaguemont, L. Jin, G. Qiao, M. Berecibar, and J. Van Mierlo, *Energies*, **12**, 4031 (2019).
43. N. Nieto, L. Díaz, J. Gastelurrutia, I. Alava, F. Blanco, J. Carlos Ramos, and A. Rivas, *J. Electrochem. Soc.*, **160**, A212 (2013).
44. N. Nieto, L. Díaz, J. Gastelurrutia, F. Blanco, J. C. Ramos, and A. Rivas, *Journal of Power Sources*, **272**, 291 (2014).
45. L. Martín-Martín, J. Gastelurrutia, N. Nieto, J. C. Ramos, A. Rivas, and I. Gil, *Applied Thermal Engineering*, **102**, 1081 (2016).
46. K. S. Ng, C. S. Moo, Y. P. Chen, and Y. C. Hsieh, *Applied Energy*, **86**, 1506 (2009).
47. S. Farhad and A. Nazari, *International Journal of Energy Research*, **43**, 931 (2019).
48. H. Maleki, S. A. Hallaj, J. R. Selman, R. B. Dinwiddie, and H. Wang, *J. Electrochem. Soc.*, **146**, 947 (1999).
49. T. W. Lee, *Thermal and Flow Measurements* (CRC Press, Boca Raton, FL) (2008).